Mechanisms of superhydrophobicity on hydrophilic substrates

2007 J. Phys.: Condens. Matter 19 356002

(http://iopscience.iop.org/0953-8984/19/35/356002)

IOP PUBLISHING JOURNAL OF PHYSICS: CONDENSED MATTER

J. Phys.: Condens. Matter **19** (2007) 356002 (12pp) doi:10.1088/0953-8984/19/35/356002

Mechanisms of superhydrophobicity on hydrophilic substrates

Jian-Lin Liu[1], **Xi-Qiao Feng**[1], **Gangfeng Wang**[2] **and Shou-Wen Yu**[1]

[1] Department of Engineering Mechanics, Tsinghua University, Beijing 100084, People's Republic of China
[2] Department of Engineering Mechanics, Xi'an Jiaotong University, Xi'an 710049, People's Republic of China

E-mail: fengxq@tsinghua.edu.cn

Received 29 January 2007, in final form 6 June 2007
Published 27 July 2007
Online at stacks.iop.org/JPhysCM/19/356002

Abstract

Surface microstructures of solids play a significant role in producing superhydrophobic surfaces. In the present paper, the Cassie–Baxter and Wenzel models on a rough substrate are examined from the viewpoints of geometry and energy. The result shows that if the air beneath a droplet on a sinusoidal substrate is open to the atmosphere, the superhydrophobic state can exist only when the substrate is hydrophobic, and that the geometric parameters of the microstructure have a great influence on the wetting behavior. Two mechanisms that may lead to a superhydrophobic property from a hydrophilic substrate are addressed. Firstly, for closed or airproof microstructures (e.g. honeycomb structures), a negative Laplace pressure difference caused by the trapped air under the drop can keep the balance of the liquid/vapor interface. Secondly, some special topologies of surface structures satisfying a certain geometric condition may also lead to the formation of a Cassie–Baxter state even if the microstructures are open to the air. Therefore, some surface morphologies may be designed to obtain superhydrophobic properties on hydrophilic surfaces. The present study is also helpful to understand some superhydrophobic phenomena observed in experiments and in nature.

(Some figures in this article are in colour only in the electronic version)

1. Introduction

Most wetting phenomena of solid materials are not only dependent upon their chemical compositions [1, 2] but also closely related to the micro- and/or nano-structures on their surfaces [3–6]. For example, the leaves of such plants as lotus and Lady's Mantle can keep off raindrops and dust due to the micro/nano-morphology of their surfaces, and this phenomenon is often referred to as the 'self-cleaning effect' or 'lotus effect' [7–9]. Such creatures as water

striders and water spiders can stand, walk and jump freely on still or even flowing water because their legs with micro- and nano-structures can produce a high superhydrophobic force to propel their bodies without being wetted [10–12]. Superhydrophobic surfaces have various applications in industry, e.g. self-cleaning paints and glass windows [13]. Much attention has been paid to mimic the microstructures of biological materials to get ultrahydrophobic properties [14–22].

The Wenzel model [23], the Cassie–Baxter model [24] and several other approximate theoretical models [25] have been established to predict the macroscopic contact angle of a liquid droplet on a rough surface. Among others, the Wenzel model assumes that the liquid wets the whole rough substrate, while the Cassie–Baxter model assumes that the droplet partially wets the rough substrate due to the trapped air in the microstructures. Carbone *et al* [26] derived the critical amplitude of a sinusoidal substrate corresponding to the transition between the two models. Johnson and Dettre [27] investigated numerically the roughness effect on the wettability of a sinusoidal surface and found that the energy barriers between two metastable states of a drop are of utmost importance in determining the magnitude of contact angle hysteresis. Quere *et al* [28–30] performed a series of experiments to investigate the transitions between the Wenzel model and the Cassie–Baxter model caused by a threshold of pressure. However, there is a lack of investigation on the quantitative dependence relationship of the macroscopically effective contact angle on the microstructure parameters of surface roughness. Therefore, it is still a puzzling issue to determine which model should be employed to calculate the contact angle for a specified surface microstructure.

It was generally thought that all superhydrophobic surfaces result from originally hydrophobic substrates with surface microstructures. However, some recent reports demonstrated that roughness can also lead to a superhydrophobic contact angle on a hydrophilic substrate. For example, the leaves of Lady's Mantle show superhydrophobic properties owing to the elasticity of the hydrophilic hairs on the hydrophilic leaves [8, 9]. Herminghaus [31] found that self-affine topologies of surface roughness may render a superhydrophobic state no matter whether the substrate is hydrophilic or hydrophobic. Hosono *et al* [16] showed that a contact angle of up to 178° may be obtained on a rough substrate with the original contact angle of only about 70°. Feng *et al* [32] created a superhydrophobic surface with a macroscopic contact angle of 171° from a substrate coated with PVA nanofibers with a contact angle of 72°. Similarly, Zhu *et al* [33] produced a rough PHBV surface with a macroscopic contact angle of 158.1°, though the Young's contact angle of smooth PHBV is only 75.9°. The above results have been explained with Cassie–Baxter model by assuming a small value of f, which denotes the fraction of the wetted solid area to the total area under the droplet. However, it is as yet unclear as to how the liquid/vapor interface is pinned on the microstructures or, in other words, how the value of f should be determined.

This paper aims to analyze how the microstructures affect the wetting models and to determine the conditions under which a specified surface morphology can lead to a superhydrophobic property. The outline of this paper is as follows. In section 2, the validation scopes of the Cassie–Baxter model and the Wenzel model on a sinusoidal substrate are discussed from the viewpoints of geometry and energy. In section 3, the case of an airproof sinusoidal hydrophilic substrate is considered to demonstrate that the negative Laplace pressure difference across the liquid/vapor interface of the trapped air blocked under the drop may cause the Cassie–Baxter state. In section 4, the Cassie–Baxter state of a hydrophilic substrate open to the air is studied, and some possible topologies of the microstructures are designed. Only two-dimensional problems will be considered in this paper, though the presented method can be extended to three-dimensional cases and the obtained conclusions also hold, at least qualitatively, for three-dimensional surface microstructures.

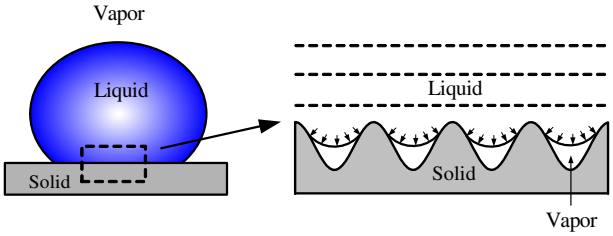

Figure 1. Cassie–Baxter state of a droplet on a substrate with sinusoidal microstructure.

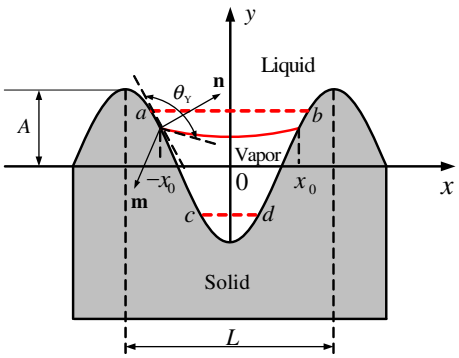

Figure 2. The geometry of the liquid/vapor interface of a droplet on a sinusoidal substrate. The Cassie–Baxter model may hold on a hydrophobic sinusoidal surface with a larger value of A/L.

2. Cassie–Baxter and Wenzel models on a rough substrate

2.1. Geometric analysis

First, let us consider a droplet located on a solid with sinusoidal surface microstructures whose characteristic sizes are much smaller than that of the liquid droplet, as shown in figure 1. The shape function of the solid surface is expressed as

$$y(x) = -A\cos(kx), \tag{1}$$

where A is the roughness amplitude, $k = 2\pi/L$ the wavenumber, and L the wavelength. The local contact state of the solid/liquid/vapor interface is shown in figure 2, where the air between the liquid and the substrate is open to the atmosphere via the interconnecting microstructure. Such a state is called the Cassie–Baxter model (or composite model). Refer to a Cartesian coordinate system (o-xy). At the triple contact point $x = -x_0$, one has the Young's equation [34]

$$\gamma_{\mathrm{SV}} - \gamma_{\mathrm{SL}} = \gamma\cos\theta_{\mathrm{Y}}, \tag{2}$$

where γ_{SV}, γ_{SL} and γ denote the surface tensions of the solid/vapor, solid/liquid and liquid/vapor interfaces, respectively, and θ_{Y} is the Young's contact angle of a smooth substrate. Since the characteristic sizes L and A of the substrate roughness are much smaller than that of the liquid drop, it is reasonable to assume that the liquid/vapor interface within a period of roughness has an arc shape written as

$$x^2 + (y - y^*)^2 = R^2, \tag{3}$$

where R is the radius of the arc, and y^* is the vertical coordinate of the circle origin. Inserting the coordinate $[x_0, -A\cos(kx_0)]$ of the solid/liquid/vapor contact point x_0, equation (3) becomes

$$y = -A\cos(kx_0) + \sqrt{R^2 - x_0^2} - \sqrt{R^2 - x^2}, \tag{4}$$

where $x_0 > 0$. Across the liquid/vapor interface, there is an over-pressure Δp (Laplace pressure difference) in the liquid with respect to the exterior pressure, which is related to the surface curvature by [35]

$$\Delta p = p_{\text{in}} - p_{\text{out}} = \frac{\gamma}{R}, \tag{5}$$

where p_{in} and p_{out} are the pressures in the liquid drop and the vapor phase, respectively. The liquid/vapor interface on such a microstructure has an invariably downward-concave meniscus shape since $\Delta p > 0$, and at the same time it must satisfy the Young's equation (2). Therefore, it is easy to see that the triple-line contact condition in the sinusoidal configuration requires the Young's contact angle $\theta_{\text{Y}} > 90°$, as shown in figure 2. From the angle of geometry, in other words, a downward-concave vapor–liquid interface cannot exist within a period of the hydrophilic sinusoidal substrate, and the liquid must wet the whole substrate region beneath the droplet. As a result of the above geometrical limitations, therefore, the Cassie–Baxter model cannot hold for such a hydrophilic substrate with a sinusoidal surface microstructure, but the Wenzel model always can.

If the substrate is hydrophobic (i.e. $90° < \theta_{\text{Y}} < 180°$), on the other hand, the liquid may either wet the whole substrate region beneath the droplet (Wenzel model) or partially contact with the substrate (Cassie–Baxter model), depending upon the Young's contact angle and the geometric parameters of the surface microstructure. The Cassie–Baxter model holds only when the contact line is in a certain range between the two dashed horizontal lines *ab* and *cd*, as shown in figure 2. Beyond this range, the Wenzel model should be used.

In figure 2, the contact angle is geometrically expressed as

$$\cos\theta_{\text{Y}} = \mathbf{m} \cdot \mathbf{n}, \tag{6}$$

where $\mathbf{m}$ and $\mathbf{n}$ are the unit vectors normal to the liquid/vapor interface and to the substrate, respectively. They are expressed as

$$\mathbf{m} = -\frac{1}{R}\left(x_0\mathbf{i} + \sqrt{R^2 - x_0^2}\,\mathbf{j}\right), \tag{7}$$

$$\mathbf{n} = \frac{kA\sin(kx_0)\mathbf{i} + \mathbf{j}}{\sqrt{1 + k^2A^2\sin^2(kx_0)}}, \tag{8}$$

where $\mathbf{i}$ and $\mathbf{j}$ are the unit vectors of the x- and y-axes, respectively. Substituting equations (7) and (8) into (6) leads to

$$\cos\theta_{\text{Y}} = -\frac{x_0 kA\sin(kx_0) + \sqrt{R^2 - x_0^2}}{R\sqrt{1 + k^2A^2\sin^2(kx_0)}}. \tag{9}$$

In the critical case of $\mathbf{m} = -\mathbf{j}$ (i.e. $R \to \infty$), equation (9) becomes

$$\cos\theta_{\text{Y}} = -\frac{1}{\sqrt{1 + k^2A^2\sin^2(kx_0)}}. \tag{10}$$

For $x_0 > 0$, the constraint condition in equation (10) is $0 < \sin(kx_0) = -\frac{1}{kA}\tan\theta_{\text{Y}} < 1$. Thus, the Young's contact angle θ_{Y} should be in the range of $\pi - \arctan(kA) \leqslant \theta_{\text{Y}} < \pi$. The solutions of equation (10) correspond to two horizontal critical lines with $R \to \infty$, which are formulated as

$$x_0^{(1)} = -\frac{1}{k}\arcsin\left(\frac{\tan\theta_{\text{Y}}}{kA}\right), \qquad x_0^{(2)} = \frac{\pi}{k} + \frac{1}{k}\arcsin\left(\frac{\tan\theta_{\text{Y}}}{kA}\right), \tag{11}$$

respectively. For $\theta_{\text{Y}} = 120°$ and the non-dimensional amplitude $\tilde{A} = A/L = 1/3$, for example, it is obtained that $\tilde{x}_0^{(1)} = x_0^{(1)}/L = 0.155$ and $\tilde{x}_0^{(2)} = x_0^{(2)}/L = 0.345$. Then the Cassie–Baxter

model holds only when the triple contact point is located in the range of $\tilde{x}_0^{(1)} < \tilde{x}_0 < \tilde{x}_0^{(2)}$. When $\tilde{x}_0 \to x_0^{(1)}$ or $\tilde{x}_0 \to x_0^{(2)}$, the radius of the liquid/vapor interface tends to be infinite and, correspondingly, the Laplace pressure difference in equation (5) approaches zero. From the viewpoint of geometry, therefore, a necessary condition for the Cassie–Baxter model to hold is that equation (10) has two unequal solutions and the triple contact point is pinned between them. If equation (10) has only one solution of x_0 or has no solution, the Cassie–Baxter model cannot be used. By this geometrical consideration, one may approximately determine whether the Wenzel model or the Cassie–Baxter should be adopted for a surface with specified microstructure. Qualitatively speaking, the Cassie–Baxter model is favorably valid when the roughness is very acute, while the Wenzel model may hold when the microstructure is relatively flat. Further discussions will be given below.

2.2. Energetic analysis

Besides the geometric limitations, the validation of the Cassie–Baxter model is further constrained by the energy relation. The surface energy within a period of roughness, which is equal to the summation of the energies of the solid/liquid and liquid/vapor interfaces within this period, is expressed as

$$L(\gamma_{\mathrm{SL}}^{\mathrm{eCB}} - \gamma_{\mathrm{SV}}^{\mathrm{eCB}}) = 2(\gamma_{\mathrm{SL}} - \gamma_{\mathrm{SV}}) \int_{x_0}^{L/2} \sqrt{1 + k^2 A^2 \sin^2(kx)}\, \mathrm{d}x + 2\gamma R \arcsin \frac{x_0}{R}, \tag{12}$$

where $\gamma_{\mathrm{SL}}^{\mathrm{eCB}}$ and $\gamma_{\mathrm{SV}}^{\mathrm{eCB}}$ are the effective surface tensions on the solid/liquid and liquid/vapor interfaces, respectively. They satisfy the generalized Young's equation:

$$\gamma_{\mathrm{SV}}^{\mathrm{eCB}} - \gamma_{\mathrm{SL}}^{\mathrm{eCB}} = \gamma \cos\theta_{\mathrm{CB}}, \tag{13}$$

where θ_{CB} is the macroscopic Cassie–Baxter contact angle. Substituting equations (2) and (13) into (12), one has the Cassie–Baxter equation

$$\cos\theta_{\mathrm{CB}} = 2\cos\theta_{\mathrm{Y}} \int_{\tilde{x}_0}^{1/2} \sqrt{1 + (2\pi\tilde{A})^2 \sin^2(2\pi\tilde{x})}\, \mathrm{d}\tilde{x} - 2\tilde{R} \arcsin \frac{\tilde{x}_0}{\tilde{R}}, \tag{14}$$

where $\tilde{x} = x/L$, $\tilde{y} = y/L$, $\tilde{x}_0 = x_0/L$ and $\tilde{R} = R/L$.

Similar to equation (12), the energy equivalence relation of the Wenzel model reads

$$L(\gamma_{\mathrm{SL}}^{\mathrm{eW}} - \gamma_{\mathrm{SV}}^{\mathrm{eW}}) = 2(\gamma_{\mathrm{SL}} - \gamma_{\mathrm{SV}}) \int_{0}^{L/2} \sqrt{1 + k^2 A^2 \sin^2(kx)}\, \mathrm{d}x, \tag{15}$$

where $\gamma_{\mathrm{SL}}^{\mathrm{eW}}$ and $\gamma_{\mathrm{SV}}^{\mathrm{eW}}$ are the effective surface tensions on the solid/liquid and solid/vapor interfaces, respectively, which also satisfy the generalized Young's equation

$$\gamma_{\mathrm{SV}}^{\mathrm{eW}} - \gamma_{\mathrm{SL}}^{\mathrm{eW}} = \gamma \cos\theta_{\mathrm{W}}, \tag{16}$$

with θ_{W} being the macroscopic Wenzel contact angle. Substituting equations (2) and (16) into (15), one has the Wenzel equation

$$\cos\theta_{\mathrm{W}} = 2\cos\theta_{\mathrm{Y}} \int_{0}^{1/2} \sqrt{1 + (2\pi\tilde{A})^2 \sin^2(2\pi\tilde{x})}\, \mathrm{d}\tilde{x}. \tag{17}$$

In addition, the Cassie–Baxter model and the Wenzel model should be constrained by

$$\cos\theta_{\mathrm{CB}} > -1, \qquad \cos\theta_{\mathrm{W}} > -1, \tag{18}$$

which can be rewritten respectively as

$$-2\cos\theta_{\mathrm{Y}} \int_{\tilde{x}_0}^{1/2} \sqrt{1 + (2\pi\tilde{A})^2 \sin^2(2\pi\tilde{x})}\, \mathrm{d}\tilde{x} + 2\tilde{R} \arcsin \frac{\tilde{x}_0}{\tilde{R}} < 1, \tag{19}$$

$$-2\cos\theta_{\mathrm{Y}} \int_{0}^{1/2} \sqrt{1 + (2\pi\tilde{A})^2 \sin^2(2\pi\tilde{x})}\, \mathrm{d}\tilde{x} < 1. \tag{20}$$

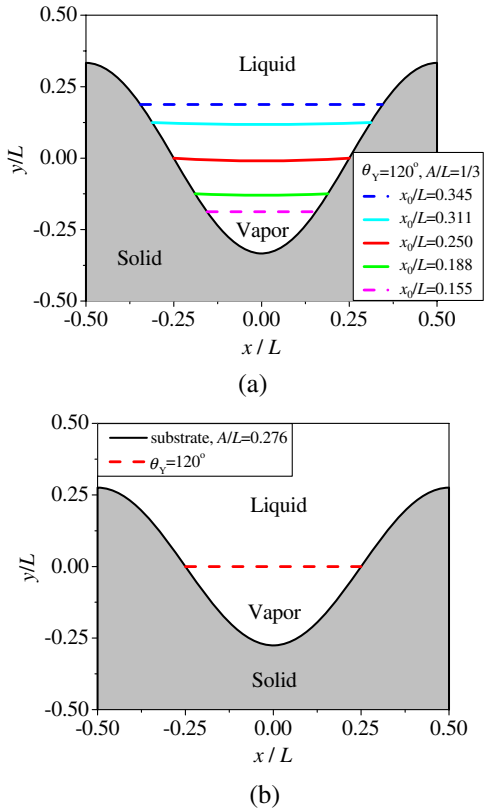

Figure 3. The shapes of the liquid/vapor interfaces with different triple-point positions, where we take (a) $\theta_Y = 120°$, $A/L = 1/3$, and (b) $\theta_Y = 120°$, $A/L = 0.276$.

Condition (20) for the Wenzel model requires that the non-dimensional amplitude $\tilde{A} = A/L$ cannot be too large. If $\theta_Y = 120°$, for example, the Wenzel model can be used only when $2\pi\tilde{A} < 2.6$. Otherwise, inequality (20) cannot be satisfied and the system tends to the Cassie–Baxter model.

On the other hand, even though the triple line is located in the range of $\tilde{x}_0^{(1)} < \tilde{x}_0 < \tilde{x}_0^{(2)}$ (that is, the geometrical condition for the Cassie–Baxter model is satisfied), the Cassie–Baxter model cannot be used if inequality (19) is not met. It is easy to see that if $\tilde{x}_0$ is too small the left term of inequality (19) will be too large and in this case only the Wenzel model can be used. Roughly speaking, therefore, the Cassie–Baxter model is energetically favorably valid for a very rough surface, but it is further limited geometrically by the position of the triple contact point.

2.3. Discussion

When both the geometry condition in equation (10) and the energy condition in equation (19) are satisfied, the Cassie–Baxter model will be valid. In this case, the shape of the liquid/vapor interface can be calculated from equations (1) and (4). The liquid/vapor interfaces on a sinusoidal substrate with $A/L = 1/3$ and $\theta_Y = 120°$ are shown in figure 3(a) for a series of triple-point positions of $\tilde{x}_0 = 0.345$, 0.311, 0.250, 0.188 and 0.155. Different

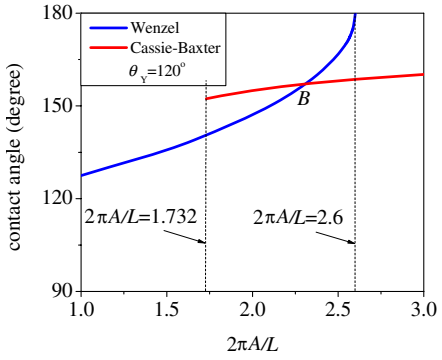

Figure 4. The macroscopic contact angles predicted by Cassie–Baxter and Wenzel models as a function of the geometric parameter $2\pi A/L$ of the microstructure, in which the air is blocked by the drop. At intersection point B, the two models predict identical contact angles.

triple-point positions produce different macroscopic contact angles according to equation (14). With the decrease in $\tilde{A}$, the two horizontal lines $\tilde{x}_0^{(1)}$ and $\tilde{x}_0^{(2)}$ approach each other. The critical state $x_0^{(1)} = x_0^{(2)} = L/4$ is reached when the corresponding non-dimensional amplitude $\tilde{A} = \sqrt{3}/(2\pi) = 0.276$, as shown in figure 3(b). When $\tilde{A}$ is smaller than 0.276, the liquid will penetrate into the whole microstructure, and then the Wenzel model will replace the Cassie–Baxter model to hold.

The contact angles of the Cassie–Baxter and the Wenzel models are calculated from equations (14) and (17) and plotted in figure 4 with respect to the variation of $\tilde{A}$, where the triple-contact line is positioned at $\tilde{x}_0 = \tilde{x}_0^{(1)}$. The result shows that only the Wenzel model is able to hold for $2\pi\tilde{A} < \sqrt{3}$ and only the Cassie–Baxter model is valid when $2\pi\tilde{A} > 2.6$. In the range of $\sqrt{3} < 2\pi\tilde{A} < 2.6$, both the models are geometrically possible, one of which corresponds to a stable and energetically favorable state and the other a metastable state. The curves corresponding to the two models have an intersection point B (figure 4), at which the two models predict the same macroscopic contact angle and, in other words, the Cassie–Baxter and the Wenzel states have an identical value of interface energy [30, 36]. This intersection point can be determined from $\theta_W = \theta_{CB}$, that is,

$$\cos\theta_Y \int_{\tilde{x}_0}^{1/2} \sqrt{1 + (2\pi\tilde{A}_C)^2 \sin^2(2\pi\tilde{x})}\, d\tilde{x} - \tilde{R} \arcsin\frac{\tilde{x}_0}{\tilde{R}} = \cos\theta_Y \int_0^{1/2} \sqrt{1 + (2\pi\tilde{A}_C)^2 \sin^2(2\pi\tilde{x})}\, d\tilde{x}, \tag{21}$$

where $\tilde{A}_C$ is the critical non-dimensional amplitude at intersection point B. For $\theta_Y = 120°$, one has $2\pi\tilde{A}_C = 2.3$. In comparison with the contact angle θ_{CB} predicted by the Cassie–Baxter model, the contact angle θ_W predicted by the Wenzel model is smaller in the range of $\sqrt{3} < 2\pi\tilde{A} < 2.3$ but larger in the range of $2.3 < 2\pi\tilde{A} < 2.6$. In the former case, the Wenzel state is stable and the Cassie–Baxter state is metastable, while in the latter case, the Cassie–Baxter model is stable and the Wenzel model is metastable.

3. Superhydrophobicity on closed microstructure

The above discussion is based on the assumption that the microstructure of the substrate is open to the air. In this case, a superhydrophobic state results only from the hydrophobic

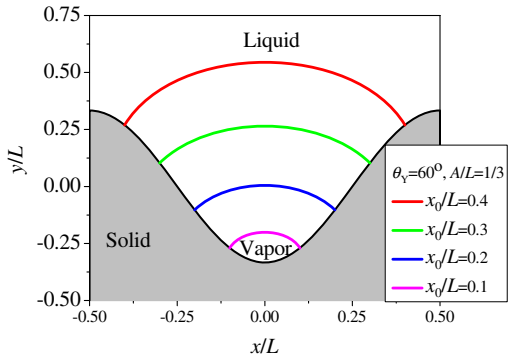

Figure 5. The shapes of the liquid/vapor interfaces with different triple-point coordinates in a closed or airproof microstructure, where $\theta_Y = 60°$ and $A/L = 1/3$.

substrate. In order to get a superhydrophobic state on a hydrophilic substrate, the conditions of the Cassie–Baxter model must be met since the Wenzel model predicts that the microstructure always amplifies the hydrophilicity of the hydrophilic substrate. One possible mechanism to achieve a hydrophobic property on a hydrophilic surface is attributed to the trapped air within the microstructure, which is isolated from the atmosphere by the liquid drop. Under this condition, the liquid/vapor interface may keep a balance due to a negative Laplace pressure difference across the interface. For a hydrophilic substrate with airproofed sinusoidal surface microstructures (e.g. honeycomb microstructures), therefore, the liquid/vapor interface may be convex and then the Cassie–Baxter model may be attained. In this case, the boundary condition is still expressed as equation (9), but the corresponding Young's contact angle $\theta_Y < 90°$.

For a hydrophilic surface with trapped air in the microstructure, the Cassie–Baxter model holds. Correspondingly, the shape function of the liquid/vapor interface is expressed as

$$y = y^* + \sqrt{R^2 - x^2}, \tag{22}$$

where y^* is the longitudinal coordinate of the circle center. Substituting the coordinate $[x_0, -A\cos(kx_0)]$ into equation (22), one has

$$y = -A\cos(kx_0) - \sqrt{R^2 - x_0^2} + \sqrt{R^2 - x^2}. \tag{23}$$

For several specified values of the triple-point locations $\tilde{x}_0 = 0.4$, 0.3, 0.2 and 0.1, the corresponding meniscus shapes are shown in figure 5, where we set $\theta_Y = 60°$. It is seen that different contact positions of the triple line can be achieved with the variation of the Laplace pressure difference induced by the trapped air. Thus the negative Laplace pressure difference of the trapped air may produce a superhydrophobic state, whose macroscopic contact angle can be predicted by the Cassie–Baxter model, as shown in figure 6. It is found that with the increase in the absolute value of the negative Laplace pressure difference, the parameter $\tilde{x}_0$ becomes larger and, correspondingly, the macroscopic contact angle increases. When $\tilde{x}_0$ is sufficiently large, a high contact angle of $\theta_Y = 150°$ can be attained on a hydrophilic substrate with $\theta_Y = 60°$. In reality, such a physical mechanism has been applied by Otten and Herminghaus [8] to produce superhydrophobic surfaces.

4. Superhydrophobicity on special surface microstructures

Besides the trapped air in the closed structures, there exist some other physical mechanisms (e.g. some special geometrical microstructures, and effect of elasticity) that may lead to

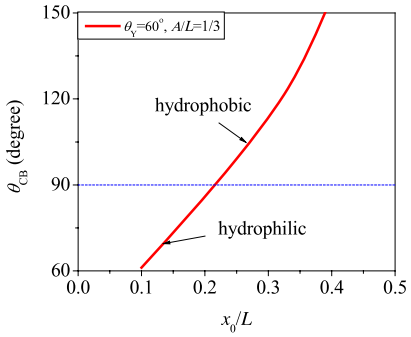

Figure 6. The macroscopic contact angle predicted by the Cassie–Baxter model as a function of the triple-point location, where we take $\theta_Y = 60°$ and $A/L = 1/2$ for example.

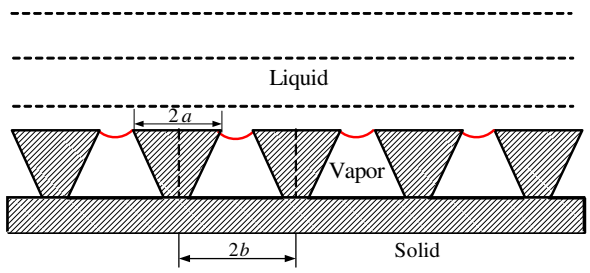

(a)

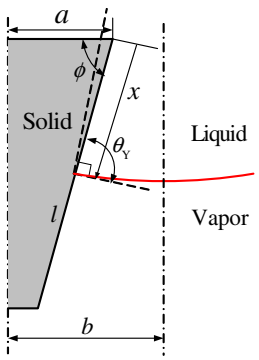

(b)

Figure 7. (a) A droplet on a substrate with surface microstructure consisting of trapezoid pillars, where $2a$ is the width of the top side of the trapezoid, and $2b$ the distance between two neighboring trapezoids. (b) The liquid/vapor interface geometry between two neighboring trapezoids, where l is the length of the inclined side, ϕ the angle measured from the top to the inclined side, and x the length of the solid/liquid interface.

superhydrophobic properties on a hydrophilic surface. Some real surface microstructures (e.g. the leaves of the lotus, Lady's Mantle and some other plants) are not airproof, but open to the atmosphere. In this section, we derive the condition for some special microstructures that yield a superhydrophobic state on a hydrophilic substrate. An example is shown in

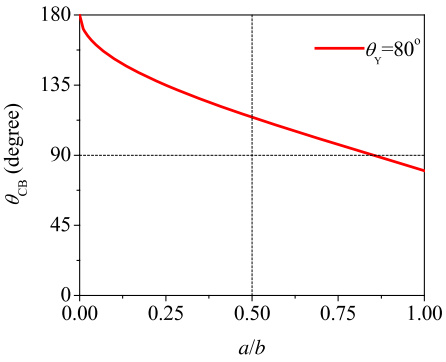

Figure 8. The macroscopic contact angle predicted by the Cassie–Baxter model as a function of the geometric parameter a/b of the microstructure, where $\theta_Y = 80°$.

figure 7(a), where the surface pattern is composed of a periodic array of trapezoids. Figure 7(b) schematizes the contact lines of the three phases. The width of the top side of the trapezoid is denoted as $2a$, the length of the inclined side l, the angle from the top to the inclined side ϕ, the distance between two neighboring trapezoid centers $2b$, and the length of the solid/liquid interface x. According to the analysis in section 2, the liquid/vapor interface is always concave. Consequently, a Cassie–Baxter state requires that $\theta_Y > \phi$. In the special case where the liquid/vapor interface is horizontal, one has $\theta_Y = \phi$.

The surface energy G within a period of roughness is equal to the summation of the energies of the solid/liquid and liquid/vapor interfaces within this period. For the microstructure in figure 7(a), the normalized surface energy $\tilde{G} = G/\gamma$ is expressed as

$$\begin{aligned}\tilde{G} &= (\gamma_{SL} - \gamma_{SV})(a + x)/\gamma + R \arcsin \frac{b - a + x\cos\phi}{R} \\ &= -\cos\theta_Y(a + x) + R \arcsin \frac{b - a + x\cos\phi}{R} \qquad (0 \leqslant x \leqslant l).\end{aligned} \tag{24}$$

The derivative of equation (24) is

$$\frac{d\tilde{G}}{dx} = -\cos\theta_Y + \frac{R\cos\phi}{\sqrt{R^2 - (b - a + x\cos\phi)^2}} > 0 \qquad (0 \leqslant x \leqslant l), \tag{25}$$

showing that the energy is a monotonically increasing function of x. So the minimum surface energy is

$$\tilde{G}_{min} = \tilde{G}(0) = -a\cos\theta_Y + R \arcsin \frac{b - a}{R} \qquad (0 \leqslant x \leqslant l). \tag{26}$$

According to the equivalence of energy, the Cassie–Baxter law is written as

$$\cos\theta_{CB} = \frac{a}{b}\cos\theta_Y - \frac{R}{b}\arcsin\frac{b - a}{R} \qquad (0 \leqslant x \leqslant l), \tag{27}$$

which shows that a superhydrophobic state can be achieved on a hydrophilic substrate. The macroscopic contact angle predicted by the Cassie–Baxter model is plotted in figure 8 as a function of a/b, where the Young's contact angle is set as a hydrophilic angle $\theta_Y = 80°$. When $R \to \infty$, the macroscopic contact angle can exceed 150°.

Based on the above understanding, some other special hydrophilic microstructures may also be designed under which the liquid/vapor interface is pinned with $\theta_Y > \phi$ and thus the Cassie–Baxter model is valid. Two examples are schematized in figure 9. Firstly, for the hydrophilic substrate with a mushroom-like microstructure in figure 9(a), the meniscus of the liquid/vapor interface is always downwards due to the Laplace pressure difference and can meet the geometric condition in equation (6) and the energy requirement in equation (19). Hence, the Cassie–Baxter state may form on such kinds of hydrophilic microstructure.

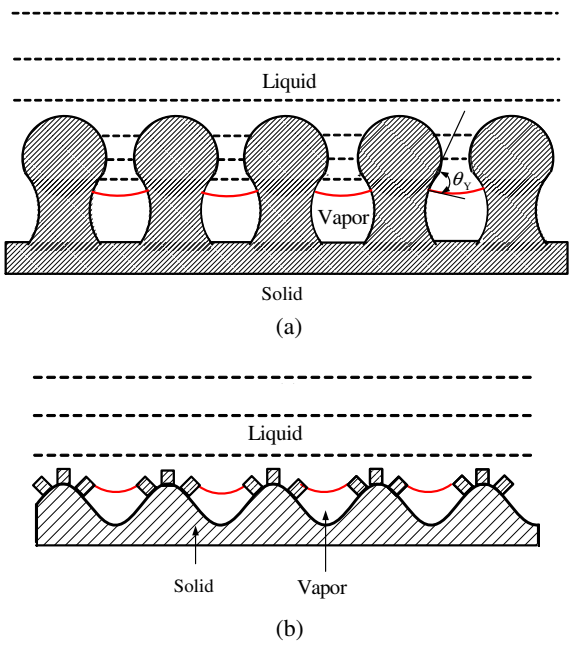

Figure 9. Two special microstructures that may produce superhydrophobic states on hydrophilic substrates: (a) mushroom-like microstructures; (b) hierarchical micro- and nano-structures.

Though a hydrophilic sinusoidal substrate cannot get a Cassie–Baxter state (as demonstrated in section 2), a hierarchical structure on a hydrophilic solid surface also leads to the formation ofa superhydrophobic state (figure 9(b)). The superhydrophobic surfaces often consist of hierarchical or fractal microstructures [7, 11, 12]. For example, the lotus leaves have two-leveled micro- and nano-structures, in which the characteristic sizes of epidermal cells (papillae) and the wax crystals are in the range of 20–50 μm and 0.5–5 μm, respectively. Due to the non-smoothness of the structures, the liquid/vapor interface may find an equilibrium configuration with a local contact angle in the range defined by the Gibbs inequality, $\theta_Y \leqslant \theta \leqslant \theta_Y + 180^\circ - \phi$, where ϕ is a characteristic angle of the microstructures (see, e.g., figure 7) [5]. Therefore, the liquid/vapor interface may be suspended on the tips of the nano-structures, resulting in a superhydrophobic property on the solid surface [26].

5. Conclusions

Surface microstructures have a significant influence on the wetting properties of solid surfaces. The mechanisms that lead to a hydrophobic state on a hydrophilic substrate have been analyzed from the viewpoints of geometry and energy. For a sinusoidal substrate, there exist three zones, namely the Wenzel zone when the non-dimensional amplitude of the sinusoidal surface is smaller than a critical value, the Cassie–Baxter zone when the non-dimensional amplitude is larger than another critical value, and the Wenzel–Cassie–Baxter zone of coexistence between them. If the air beneath the liquid drop is open to the atmosphere, the Cassie–Baxter model is unable to hold on a hydrophilic sinusoidal substrate and may hold on a hydrophobic sinusoidal substrate ($\pi/2 < \theta_Y < \pi$) satisfying certain conditions of geometry and energy. We have addressed two mechanisms to explain the superhydrophobic state stemming from a hydrophilic substrate. Firstly, the trapped air blocked in the airproof roughness may produce a negative Laplace pressure difference and lead to a superhydrophobic state on a sinusoidal hydrophilic substrate. Secondly, some special topologies of the pillars or hairs on solid substrates may

also make the Cassie–Baxter model hold and produce hydrophobic or even superhydrophobic surfaces. The obtained results may elucidate some wetting phenomena observed in experiments or in nature [16, 31–33]. Finally, it should be noted that there are some other factors (e.g. elastic deformation of substrates) that may affect the wetting properties of surfaces but are not included in the present study.

Acknowledgments

The project is supported by the National Natural Science Foundation of China (10525210, 10121202 and 10602042) and the Ministry of Education of China.

References

[1] Lipowsky R, Brinkmann M and Dimova R 2005 *J. Phys.: Condens. Matter* **17** S537
[2] Brinkmann M, Kierfeld J and Lipowsky R 2005 *J. Phys.: Condens. Matter* **17** 2349
[3] de Gennes P G, Brochard-Wyart F and Quere D 2003 *Capillarity and Wetting Phenomena: Drops, Bubbles, Pearls, Waves* (Berlin: Springer)
[4] de Gennes P G 1985 *Rev. Mod. Phys.* **57** 827
[5] Quere D 2002 *Physica* A **313** 32
[6] Liu J L, Feng X Q and Yu S W 2006 *Acta Mech. Sin.* **22** 315
[7] Neinhuis C and Barthlott W 1997 *Ann. Bot.* **79** 667
[8] Otten A and Herminghaus S 2004 *Langmuir* **20** 2405
[9] Mock U, Forster R, Menz W and Ruhe J 2005 *J. Phys.: Condens. Matter* **17** S639
[10] Hu D L, Chan B and Bush J W 2004 *Nature* **424** 663
[11] Feng X Q, Gao X F, Wu Z N, Jiang L and Zheng Q S 2007 *Langmuir* **23** 4892
[12] Gao X F and Jiang L 2004 *Nature* **432** 36
[13] Blossey R 2003 *Nat. Mater.* **2** 301
[14] Lau K K S, Bico J, Teo K B K, Chhowalla M, Amaratunga G A J, Milne W I, Mckinley G H and Gleason K K 2003 *Nano Lett.* **3** 1701
[15] Zhai L, Cebeci F C, Cohen R E and Rubner M F 2004 *Nano Lett.* **4** 1349
[16] Hosono E, Fujihara S, Honma I and Zhou H S 2005 *J. Am. Chem. Soc.* **127** 13458
[17] Jeong H E, Lee S H, Kim J K and Suh K Y 2006 *Langmuir* **22** 1640
[18] Shibuichi S, Onda T, Satoh N and Tsujii K 1996 *J. Phys. Chem.* **100** 19512
[19] Alberti G and DeSimone A 2005 *Proc. R. Soc.* A **461** 79
[20] Bico J, Thiele U and Quere D 2002 *Colloids Surf.* A **206** 41
[21] Shi F, Niu J, Liu J L, Liu F, Wang Z Q, Feng X Q and Zhang X 2007 *Adv. Mater.* at press
[22] Onda T, Shibuichi S, Satoh N and Tsujii K 1996 *Langmuir* **12** 2125
[23] Wenzel R N 1936 *Ind. Eng. Chem.* **28** 988
[24] Cassie A B D and Baxter S 1944 *Trans. Faraday Soc.* **40** 546
[25] Zheng Q S, Yu Y and Zhao Z H 2005 *Langmuir* **21** 12207
[26] Carbone G and Mangialardi L 2005 *Eur. Phys. J.* E **16** 67
[27] Johnson R E and Dettre R H 1964 *Adv. Chem. Ser.* **43** 112
[28] Bico J, Tordeux C and Quere D 2001 *Europhys. Lett.* **55** 214
[29] Ishino C, Okumura K and Quere D 2004 *Europhys. Lett.* **68** 419
[30] Lafuma A and Quere D 2003 *Nat. Mater.* **2** 457
[31] Herminghaus S 2000 *Europhys. Lett.* **52** 165
[32] Feng L, Song Y L, Zhai J, Liu B Q, Xu J, Jiang L and Zhu D B 2003 *Angew. Chem. Int. Edn* **42** 800
[33] Zhu M F, Zuo W W, Yu H, Yang W and Chen Y M 2006 *J. Mater. Sci.* **41** 3793
[34] Young T 1805 *Phil. Trans. R. Soc.* **95** 65
[35] Adamson A W 1990 *Physical Chemistry of Surfaces* (New York: Wiley)
[36] Patankar N A 2003 *Langmuir* **19** 1249